 doi:10.20944/preprints202102.0077.v1

Article

Hot box investigations of a ventilated bioclimatic wall for NZEB building façade

Dwinanto Sukamto [1], Monica Siroux [1,*] and Francois Gloriant [1]

[1] INSA Strasbourg ICUBE, University of Strasbourg; dwinanto.sukamto@insa-strasbourg.fr
INSA Strasbourg ICUBE, University of Strasbourg; monica.siroux@insa-strasbourg.fr
INSA Strasbourg ICUBE, University of Strasbourg; francois.gloriant@insa-strasbourg.fr
* Correspondence: monica.siroux@insa-strasbourg.fr; Tel.: +33-3881-447-53

Abstract: The building sector is the largest consumer of energy and there are still major scientific challenges in this field. The façade, being the interface between the exterior and interior space, plays a key role in the energy efficiency of a building. In this context, this paper focuses on a ventilated bioclimatic wall for NZEB zero energy buildings. The objective of this study is to investigate an experimental set-up based on a Hot Box allowing characterizing the thermal performances of the ventilated wall. A specific ventilated prototype and an original thermal metrology has been developed. This paper presents the ventilated prototype, the experimental set-up and experimental results on the thermal performances of the ventilated wall. The influence of the air space thickness and the air flow rate on the thermal performances of the ventilated wall is studied.

Keywords: thermal performance, ventilated bioclimatic wall, air space thickness, air flow rate, Hot Box

---

Nomenclature

E pre-heating efficiency of the ventilated wall
h convection heat transfer coefficient, $W.m^{-2}.°C^{-1}$
HR relative humidity inside the cell, %
T temperature, °C
q flux density, $W.m^{-2}$

Indices
a ambiance of the cell
in relative to the inside air temperature (hot cell)
inlet relative to the supply air temperature measured in the top of the air cavity
out relative to the outside air temperature (cold cell)
s wall surface

1. Introduction

The building sector is responsible for 40% of energy consumption in Europe [1]. Reducing the energy consumption and the emission of gases of buildings has become a priority nowadays in Europe. In this context, France is placing the construction sector at the heart of its strategy to meet this challenge [2]. Nowadays, a building must ensure low energy consumption and good environment quality. However, the building envelope is the construction element that has one of the most important impacts on the overall energy consumption of the building. These aspects generate innovative facade design [3,4]. In particular, the ventilated facade can be also a response to this approach [5].

 doi:10.20944/preprints202102.0077.v1

Architects choose the ventilated facade as an envelope solution in a wide variety of building types, climates and design configurations. The system offers a wide variety of exterior claddings and the ability to select a wide variety of materials, colors and panel sizes. In addition to the aesthetic aspect, the primary purpose of this type of façade is to protect the insulation materials by dissipating moisture.

The ventilated façade is composed of two panes, separated by a ventilated air layer. The ventilated façade can be continuous or divided into modules. The air layer forms a thermal buffer zone. The ventilation of the cavity can be natural, mechanical or both (hybrid), through openings in the external and internal skin.

For several years, publications on ventilated walls increased significantly [6, 7, 8, 9, 10, 11, 12, 13,14, 15, 16, 17]. Despite the high number of publication on ventilated walls, the influence of the air space thickness cavity on the thermal performances of the ventilated wall was little studied. The table 1 gives an overview of different study on the ventilated façade from a point of view of the air space thickness.

The objective of this study is to develop an experimental set-up able to characterize the influence of the air space thickness and the air flow rate on the thermal performances of the ventilated wall. A specific ventilated prototype and an original thermal metrology has been developed on this subject. This paper described the original set-up, the ventilated bioclimatic prototype, the instrumentations involved in the test specimen and the experimental results.

Table 1. Overview of different study on the ventilated façade

Author	Years	Sample	Air space thickness
A. Alaidroos [18]	2016	Ventilated wall	0,1 m
O. Aleksandrowicz, [19]	2018	Double skin facade	0,2 m
J. Wang [20]	2017	Triple glazed windows	0,03 m, 0,012 m
L. C. O. Souza [21]	2018	Ventilated double-skin façade	0,1 m
J. Parra [22]	2015	Ventilated double-skin façade	0,2 m, 2 m
G. Michaux [23]	2019	Triple glazed windows	0,015 m
F. Gloriant [24]	2021	Triple glazed windows	0,013 m

2. Experimental set up

2.1. Bioclimatic ventilated wall and Hot Box

The ventilated wall prototype is presented in Figure 1. This prototype consists in two walls and a ventilated air chamber (cavity between the two walls). The first wall is fixed while the second one is mobile, allowing the thickness of the ventilated cavity to be varied. These two walls are made of an aluminum alloy and polyethylene. The dimensions are 1m high, 1m wide and 3 mm thickness. Based manufacturer's data, the aluminum composite has a thermal resistance of 0.008 $m^2.K.W^{-1}$ and has low roughness with their surfaces are smooth. The ventilated air chamber is a non-hermetically cavity that participates in the supply of fresh air to the building. A convective exchange takes place in the cavity along the axis of the wall, which disturbs the radial heat flow between the interior and exterior environments (Figure 1).

Preprints (www.preprints.org) | NOT PEER-REVIEWED | Posted: 2 February 2021 doi:10.20944/preprints202102.0077.v1

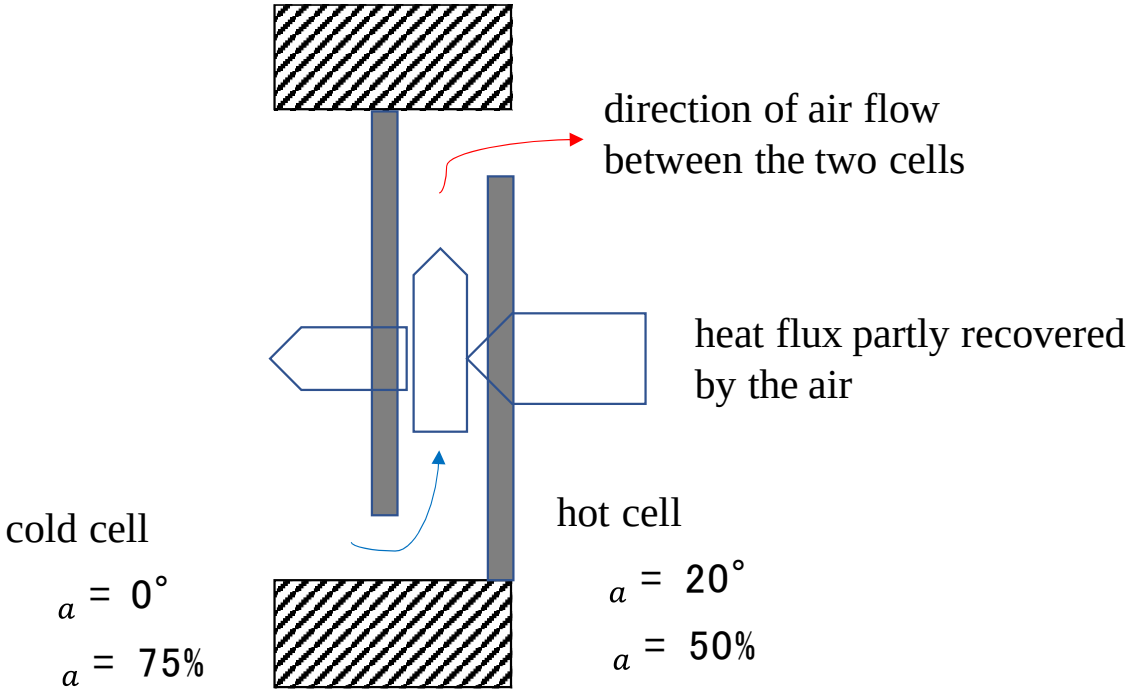

Figure 1. Ventilated wall.

The experimental study was carried out in a guarded Hot Box (Figure 2). This guarded Hot Box is a device composed of two climatic chambers chose ambiances are controlled. The first climatic chamber reproduces indoor conditions, the second reproduces outdoor conditions (Figure 2). The Hot Box is characterize by a range of temperature from -30°C to +60°C and a range of humidity from 10% to 98%. Each climatic chamber has its own refrigeration unit that allow the production of cold with a temperature accuracy of ± 2°C. Each climatic chamber has also 3 electric resistors of 2.5 kW, that allow the production of heat with a temperature accuracy of ± 3 °C. The guarded Hot Box is connected to a computer to control the temperature and humidity of each climatic chamber. These two climatic chambers are separated by a sample holder (size of 1mx1mx0.4m). One of the two chambers is mounted on slides, which allows us to access the sample holder as well as the inside of the two climatic chambers. The ventilated bioclimatic prototype is fixed in the specimen holder. A ventilation system is used to impose the air flow in the cavity. The air space thickness can be varied by moving the mobile wall.

Experiments were carried out for different configurations: variable air space thickness and variable air flow rate. The air space thickness varies from 5 mm to 85 mm. The air flow rate varies from 10 $m^3.h^{-1}$ to 30 $m^3.h^{-1}$. 50 experiments have been carried out. An overview of 25 experiments is given in Table 2.

Preprints (www.preprints.org) | NOT PEER-REVIEWED | Posted: 2 February 2021 doi:10.20944/preprints202102.0077.v1

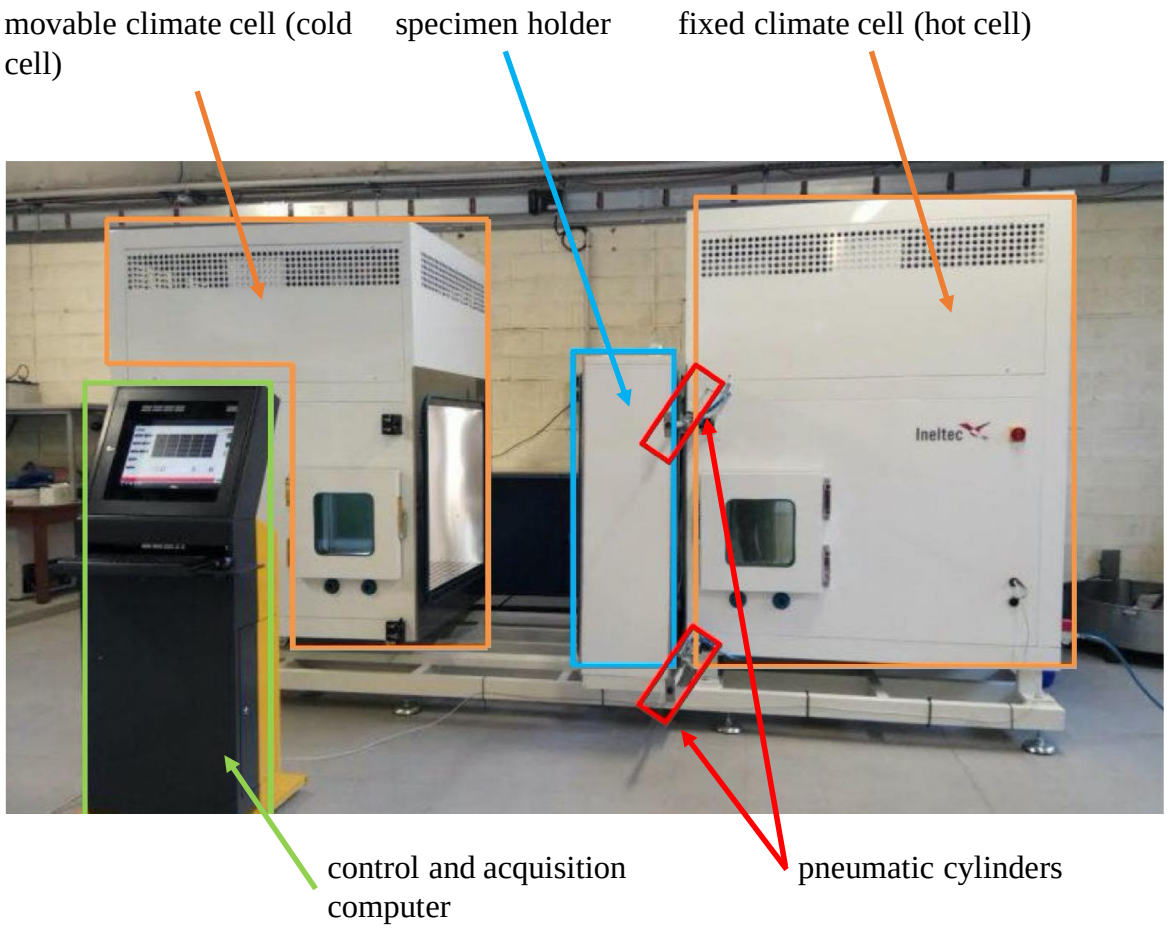

Figure 2. Hot Box.

Table 2. Overview of 25 experiments.

Test number	Air space thickness (mm)	Air flow velocity ($m^3.h^{-3}$)	Cold cell temperature T_{a1} (°C)	Hot cell temperature T_{a2} (°C)	Temperature difference between hot cell and cold cell (°C)
1	5	9,942	-4,34	15,56	19,9
2	5	19,609	-4,64	15,63	20,27
3	5	29,997	-4,45	15,82	20,27
4	10	9,936	-4,64	15,58	20,23
5	10	19,957	-4,72	15,61	20,32
6	10	29,996	-4,47	15,8	20,27
7	15	10,002	-4,61	15,58	20,19
8	15	19,999	-4,63	15,66	20,29
9	15	30,097	-4,41	15,87	20,28
10	20	9,983	-4,67	15,62	20,29
11	20	20,434	-4,66	15,64	20,29
12	20	29,84	-4,41	15,86	20,27
13	25	10,02	-4,67	15,61	20,28
14	25	20,078	-4,63	15,68	20,31

Preprints (www.preprints.org) | NOT PEER-REVIEWED | Posted: 2 February 2021 doi:10.20944/preprints202102.0077.v1

15	25	29,813	-4,43	15,87	20,3
16	30	9,900	-4,65	15,66	20,31
17	30	19,851	-4,62	15,71	20,33
18	30	29,982	-4,32	15,9	20,22
19	35	10,222	-4,65	15,63	20,28
20	35	19,893	-4,64	15,63	20,27
21	35	30,039	-4,32	15,95	20,28
22	40	8,986	-4,67	15,66	20,33
23	40	20,074	-4,61	15,74	20,35
24	40	30,046	-4,29	15,86	20,15
25	45	9,038	-4,66	15,64	20,3

2.2. Thermal metrology

The instrumentation is composed on K-type thermocouples and PT 100 probes. The Hot Box ambient temperature is measured in hot cell and cold cell with K-type thermocouples and PT-100 sensors (Hot Box sensors). The Hot Box instrumentation is presented in Figure 3. The ventilated prototype consists in two walls and an air cavity. The first wall is fixed while the second one is mobile, allowing the thickness of the ventilated cavity to be varied. The walls surface temperature is measured by 24 K-type thermocouples (12 thermocouples on the fixed wall and 12 thermocouples on the mobile wall). The position of the thermocouples is given in the Figure 4, Figure 5 and Figure 6. Thermocouples measurements are compared to that obtained using an infrared camera (FLIR T650 SC). The infrared camera is installed in the front of the wall. The area covered by the infrared camera has a surface area of 10 cm^2. The thermal flux is measured with 8 fluxmeter Captec ® (4 fluxmeter on the fixed wall and 4 flumeter on the mobile wall), allowing the estimation of heat flux on both sides of the ventilated cavity (Figure 4). The air cavity temperature is measured by 10 K-type thermocouples (4 thermocouples in the cavity, 3 thermocouples at the entrance of the cavity and 3 thermocouples at the exit of the cavity). To control the airflow velocity inside the air cavity a convergent plenum was installed (Figure 4). A fan was used to vary the airflow velocity inside the cavity. A CTV 210 hot wire anemometer from the manufacturer KIMO measures the airflow velocity. All the sensors are connected to data acquisition system Keithley 2700®. Data acquisition and processing are then carried out via the LabVIEW software (Figure 7).

The characteristics of the sensors used are given in Table 3.

Table 3 . Thermal metrology

Type	Metrologic Means	Range	Uncertainity
Air temperature	PT100	-70° C to + 200 °C	0,1 °C
	K-type Thermocouples	-75° C to + 250 °C	0,02 °C
Surface temperature	K-type Thermocouples	-75° C to + 250 °C	0,02 °C
	Infrared camera Flir T650 sc	-40° C to +150 °C	1 %
Thermal Flux	Captec Fluxmeter		5 %
Air flow velocity	Hot wire anemometer KIMO CTV 210	0-30 m/s	0.3 m/s

Preprints (www.preprints.org) | NOT PEER-REVIEWED | Posted: 2 February 2021 doi:10.20944/preprints202102.0077.v1

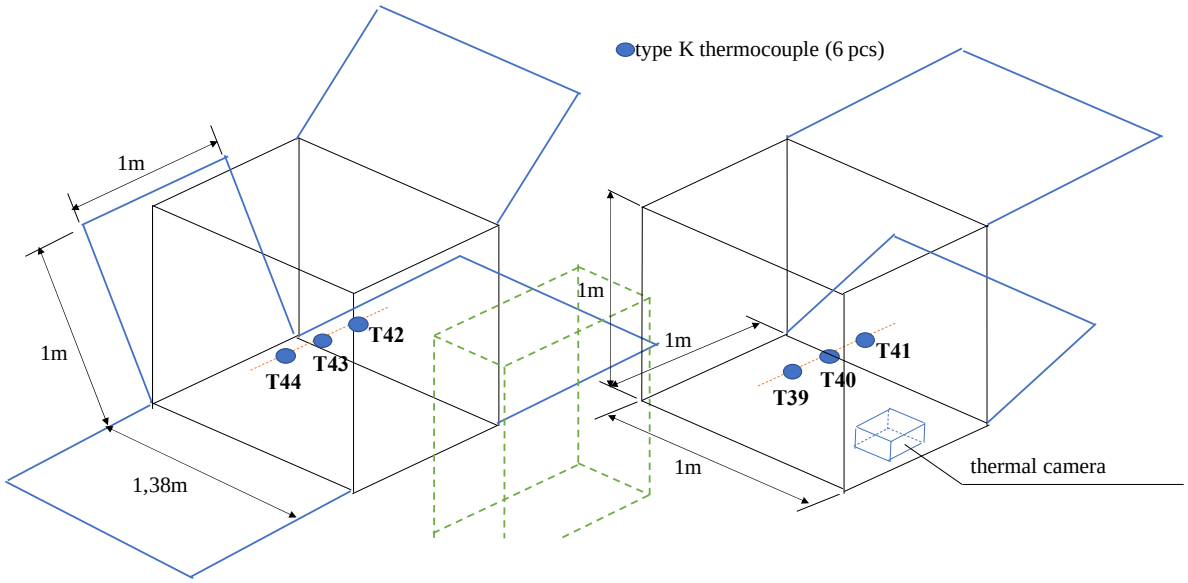

Figure 3. Hot Box instrumentation.

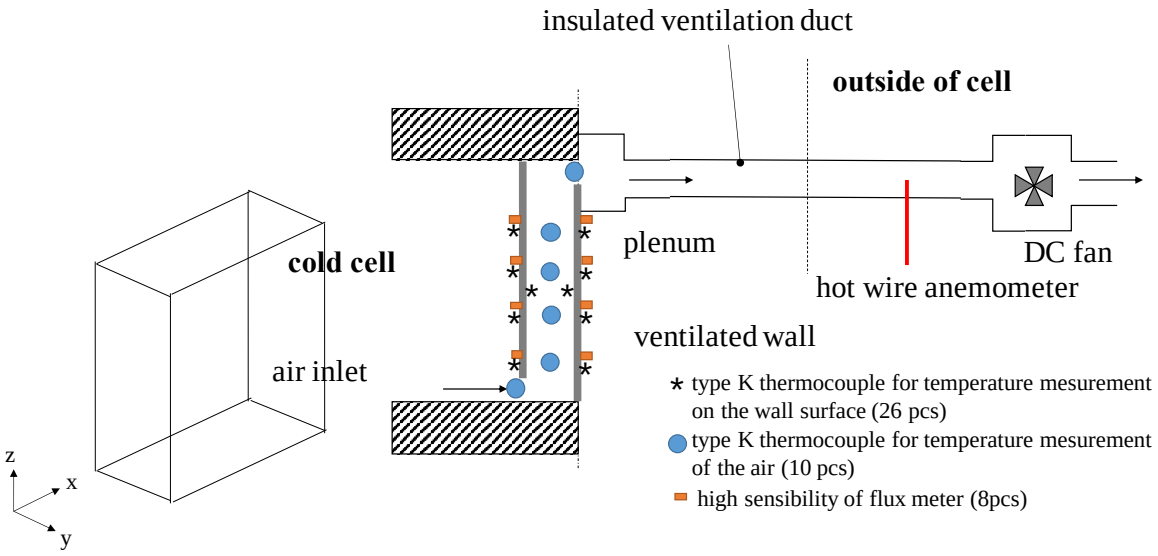

Figure 4. Ventilated wall instrumentation.

Preprints (www.preprints.org) | NOT PEER-REVIEWED | Posted: 2 February 2021 doi:10.20944/preprints202102.0077.v1

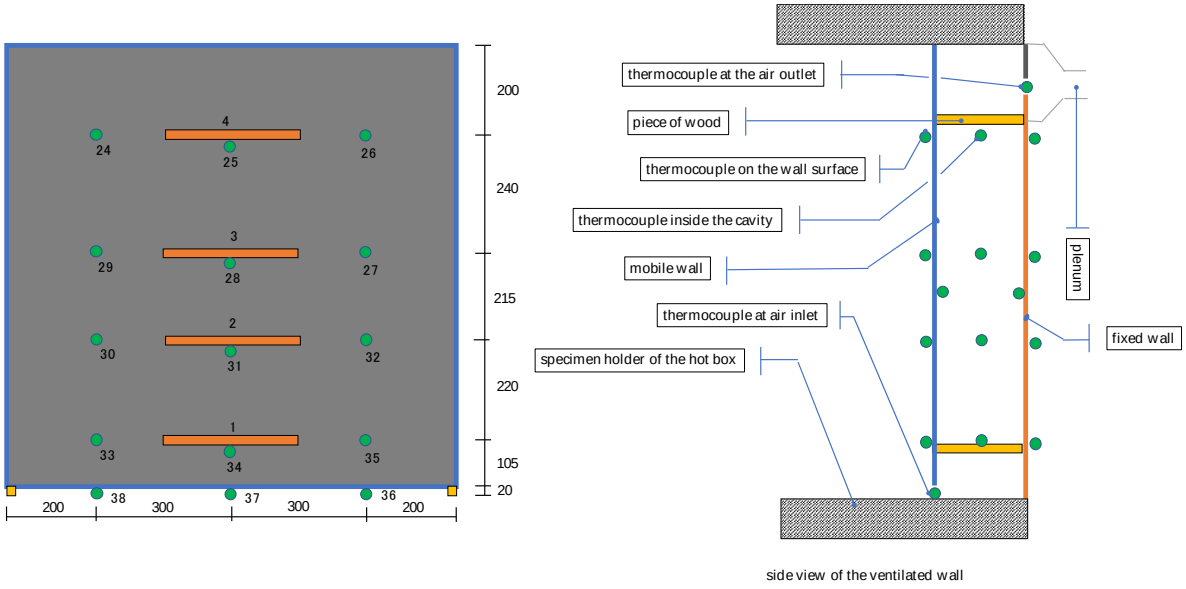

Figure 5. Mobile wall instrumentation

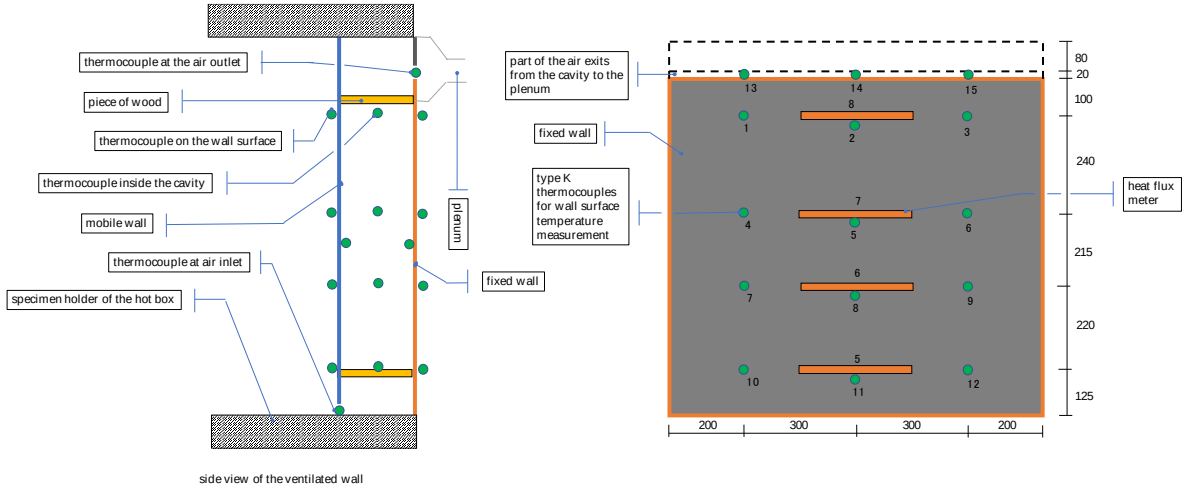

Figure 6. Fixed wall instrumentation

Preprints (www.preprints.org) | NOT PEER-REVIEWED | Posted: 2 February 2021 doi:10.20944/preprints202102.0077.v1

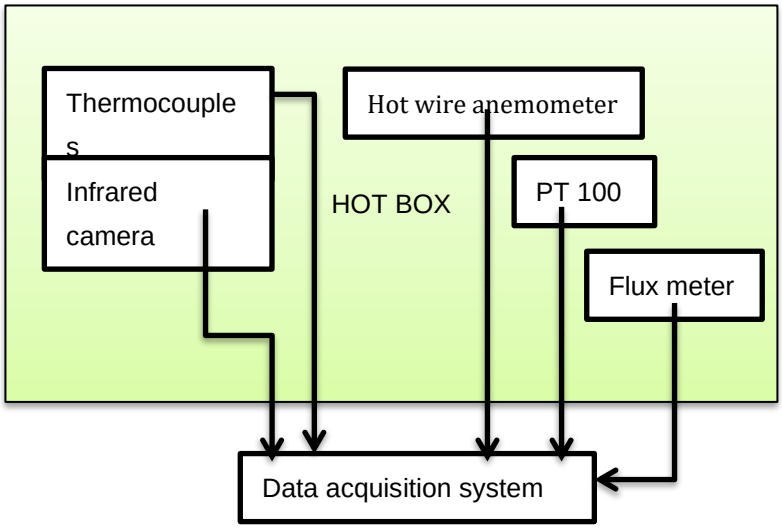

Figure 7. Data acquisition system

3. Experimental results

Experiments have been undertaken to test the Hot Box and the ventilated wall prototype. Experiments were carried out in steady state under the following conditions:

- Hot cell: ambient temperature conditions of 20°C and relative humidity 55%
- Cold cell: temperature conditions of 0°C, 75% relative humidity
- Variable airflow rate: 10 $m^3.h^{-1}$, ^{20} $m^3.h^{-1}$ and 30 $m^3.h^{-1}$
- Variable air space thickness: from 5 mm to 85 mm

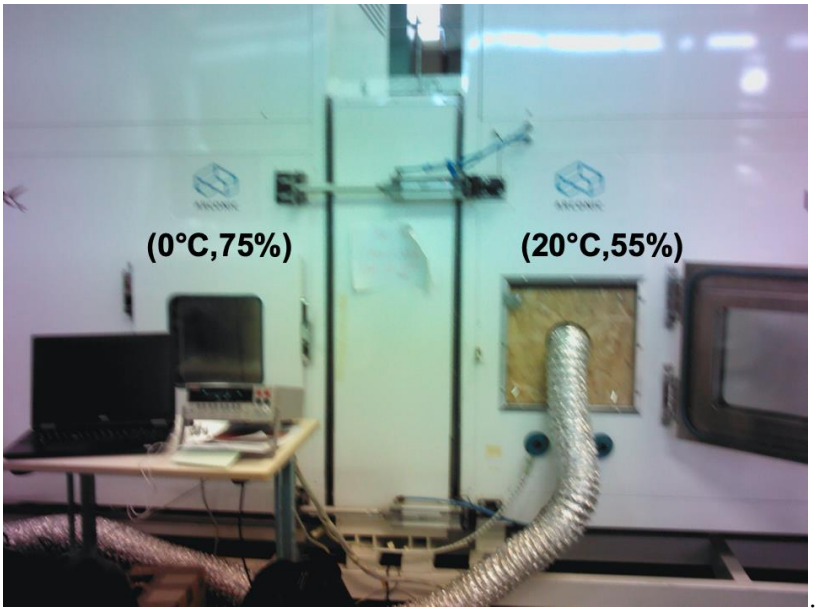

Figure 8. Experimental set-up.

3.1. Ambiant temperature

The ambient temperature was measured in both, hot cell and cold cell with K-type thermocouples and PT-100 sensors (Hot Box sensors). The temperature difference between the hot cell and cold was 20°C. This temperature difference allows obtaining a heat flux that can be measured by the correctly measured by the flux meters [25].

Under the specified conditions (20°C in the hot cell and 0°C in the cold cell), a significant difference (2.6°C for the cold cell and 4.3°C for the hot cell) can be observed between the ambient

Preprints (www.preprints.org) | NOT PEER-REVIEWED | Posted: 2 February 2021 doi:10.20944/preprints202102.0077.v1

temperature measured with the Hot Box sensor and the ambient temperature measured by our thermocouples. This difference can be explained by the fact that the cells are not watertight since an artificial air flow has been created between them. However, for standard use of the guarded hot box, there should not be any air exchange between the cells; the regulation system of the device is then disturbed.

It can be seen in Figure 9 and Figure 10 that the air temperature inside the hot box is homogenous in cold cell and hot cell. The mean air temperature is -4,6±0,05 °C for the cold cell and 15.7±0,18 °C for the hot cell.

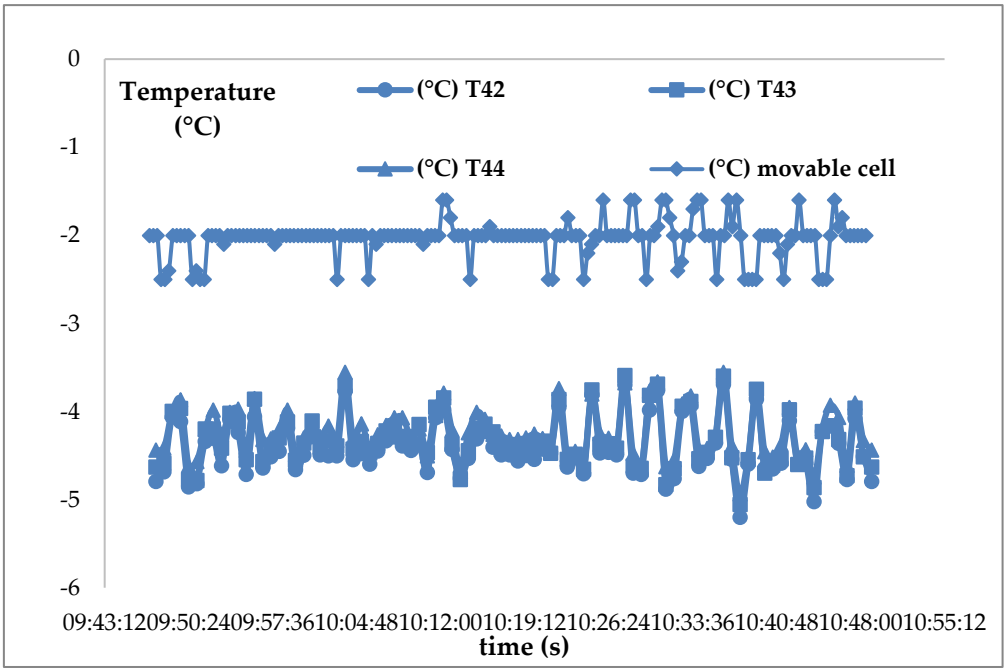

Figure 9. Ambient temperature in the cold cell.

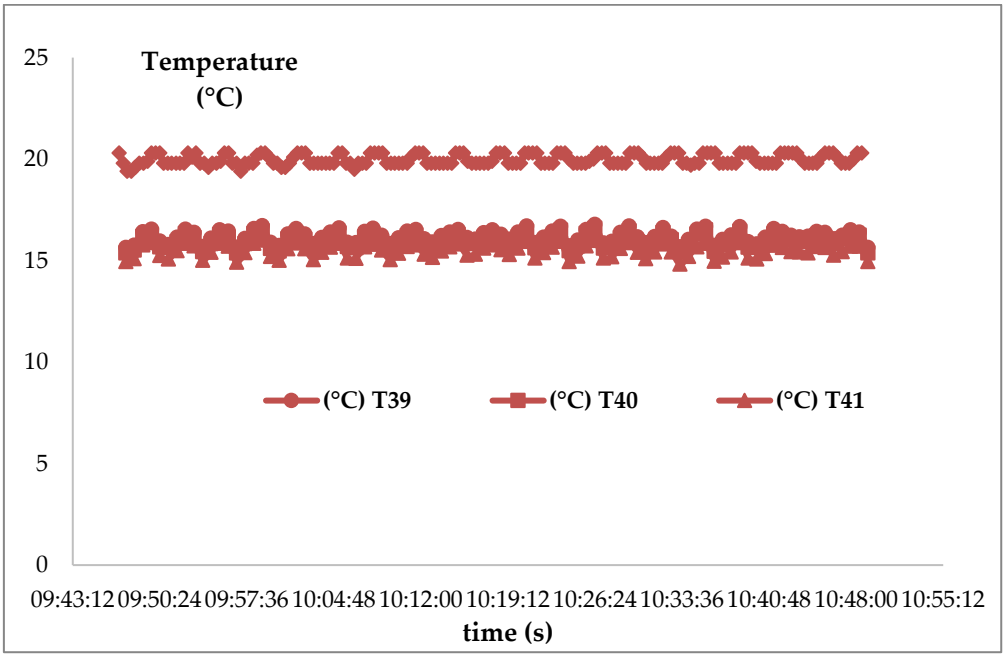

Figure 10. Ambient temperature in the hot cell.

Preprints (www.preprints.org) | NOT PEER-REVIEWED | Posted: 2 February 2021 doi:10.20944/preprints202102.0077.v1

3.2. *Surface temperatures*

Measurement of surface temperatures is done by thermocouples. Thermocouples measurements are compared to data obtained using an infrared camera (Figure 11). The area covered by the infrared camera has a surface area of 10 cm². The T8 and T5 thermocouples are located on the upper and lower part of this surface. The measurements of surface temperatures by the thermocouples are in adequacy with the measurements made by the infrared camera and confirm the reliability of the instrumentation of the walls (Figure 12).

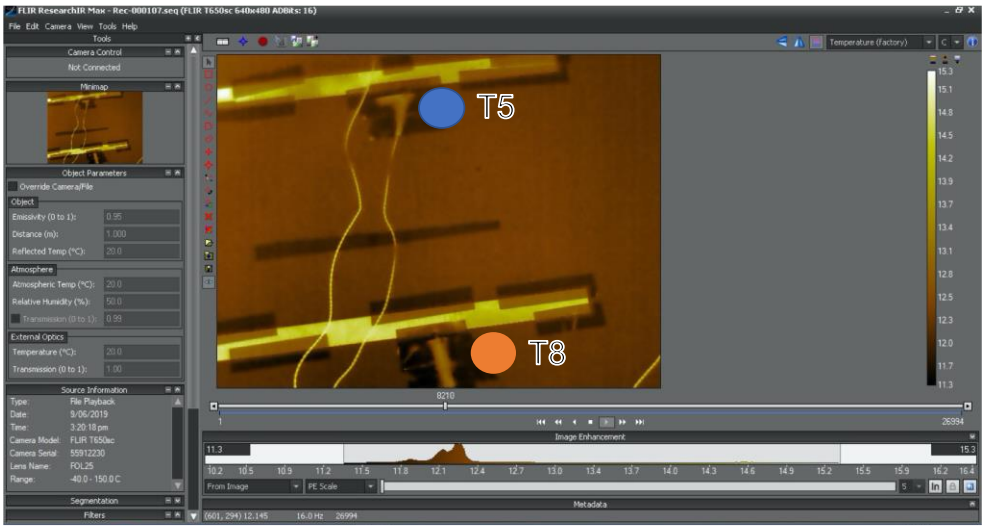

Figure 11. Surface temperature measurement by infrared camera.

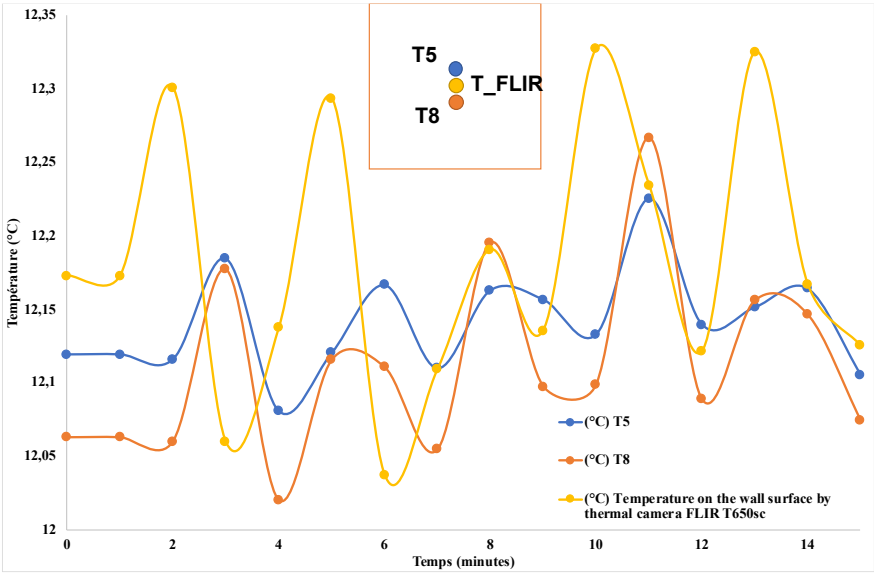

Figure 12. Surface temperature. Thermocouples and infrared camera measurements.

Preprints (www.preprints.org) | NOT PEER-REVIEWED | Posted: 2 February 2021 doi:10.20944/preprints202102.0077.v1

3.3. The convection heat transfer coefficient

The convection heat transfer coefficient is estimate from Newton's law that involved the heat flux, the ambient temperature and the wall temperature:

$$h=q/(T_s-T_a) \quad (1)$$

The heat flux, the ambient temperature and the wall temperature are measured using thermal metrology describes before. We used 2 cavity thicknesses (0.005 m and 0.01 m) and 3 airflow rate (10 $m^3.h^{-1}$, 20 $m^3.h^{-1}$ and 30 $m^3.h^{-1}$). Each sample wall is equipped with 4 fluxmeters and 4 thermocouples at different heights, it is possible to obtain 4 local estimates of the h-factor per cell. For the ambient temperature in each of the cells, a single air temperature is considered, corresponding to the average of the measurements of the 3 thermocouples installed in each cell. Figure 13 and Figure 14 shows the local convection heat transfer coefficient h in the cold cell and in the hot cell. The values of the heat transfer coefficient varies between 15 $W.m^{-2}.K^{-1}$ and 25 $W.m^{-2}.K^{-1}$. The mean value of the heat transfer coefficient is 19,9±1,3 $W.m^{-2}.K^{-1}$ for the cold cell and 18.7±2,3 $W.m^{-2}.K^{-1}$ for the hot cell. The result of the estimation of the heat transfer coefficient found good agreement with the references in the literature [26]. It can be noted that the thickness of the cavity and the airflow rate have not significant influence on the convection heat transfer coefficient value. This means that these 2 parameters have no influence on the ambiances of the 2 climate cells. On the other hand, the coefficient *h* depends on the position at which it has been calculated and it can be seen that, for a given height, the estimates of the coefficient *h* are relatively homogeneous. It can be thought that, in each of the cells, the air movements caused by the regulation system are not uniform near the walls of the sample, causing local variations in the coefficient *h*.

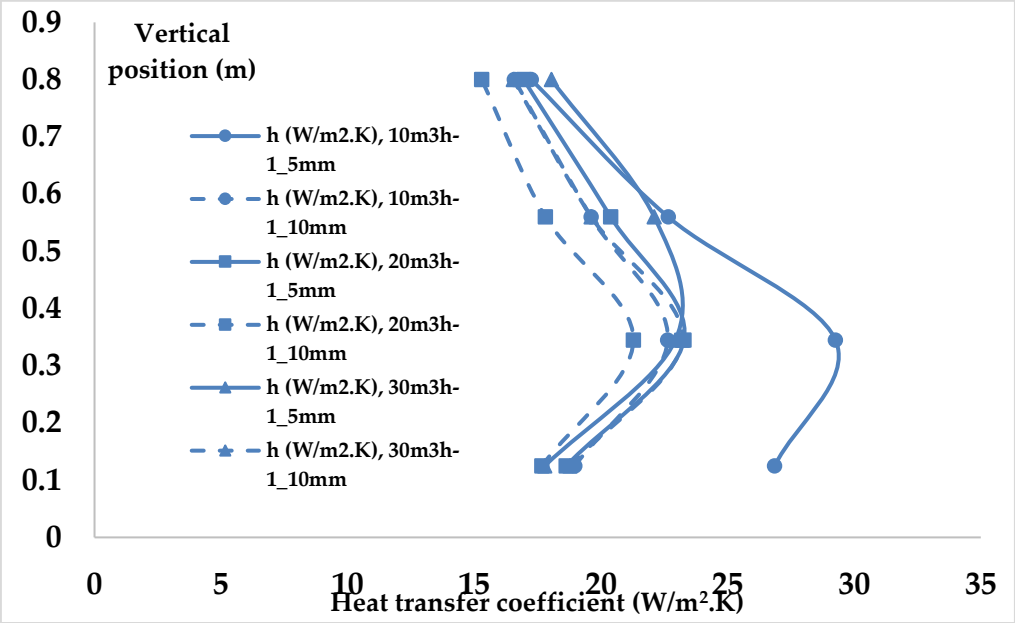

Figure 13. The local convection heat transfer coefficient in the cold cell.

Preprints (www.preprints.org) | NOT PEER-REVIEWED | Posted: 2 February 2021 doi:10.20944/preprints202102.0077.v1

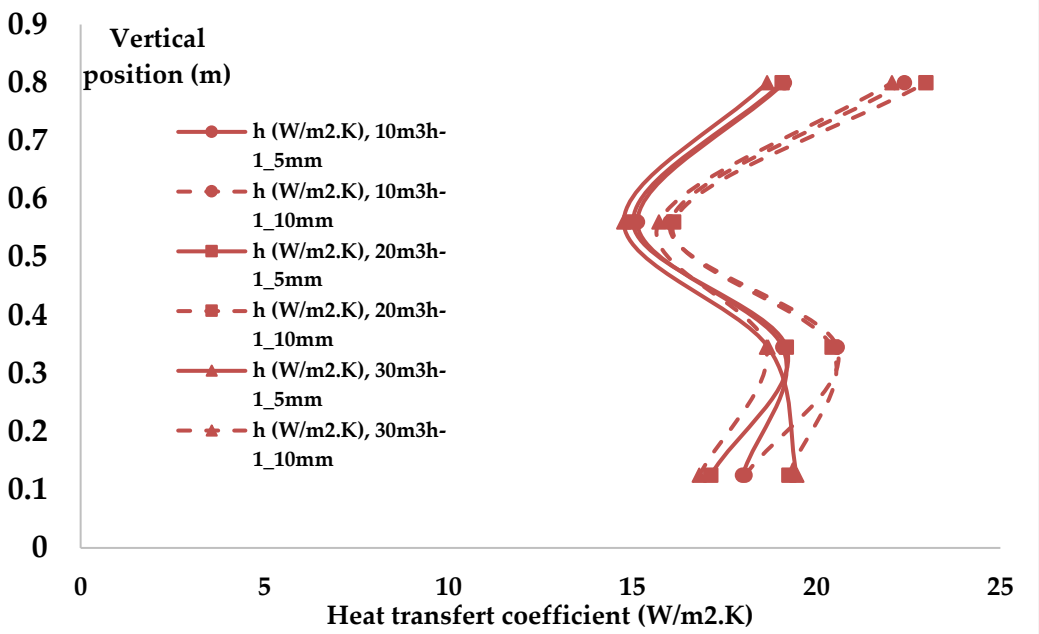

Figure 14. The local convection heat transfer coefficient in the hot cell.

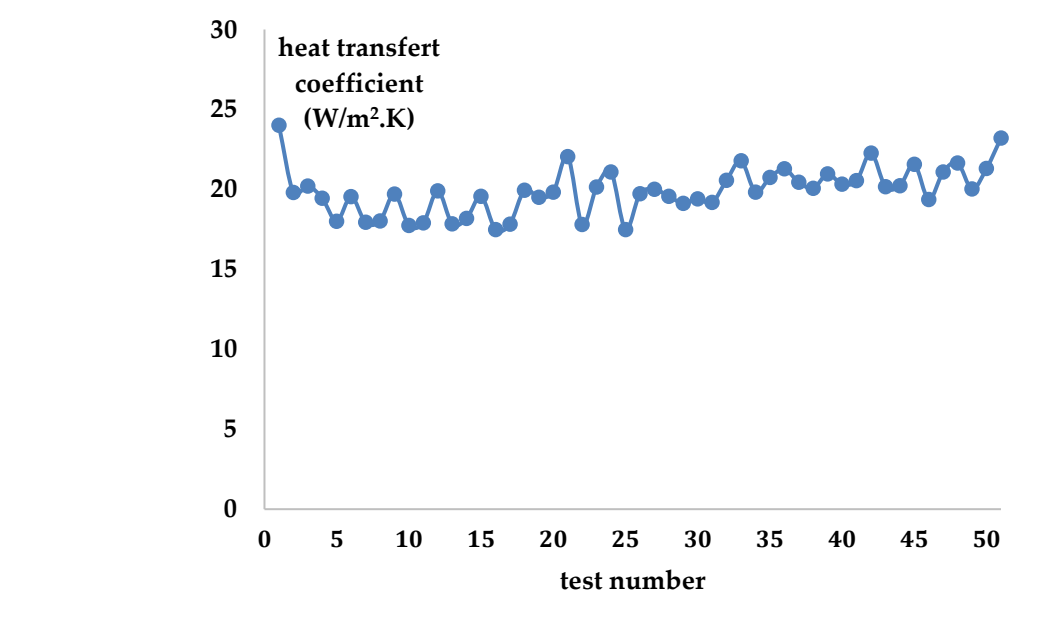

Figure 15. Estimation of the global heat transfer coefficient in the cold cell from temperatures measurements (thermocouples) and heat fluxes (flux meters measurements).

Preprints (www.preprints.org) | NOT PEER-REVIEWED | Posted: 2 February 2021 doi:10.20944/preprints202102.0077.v1

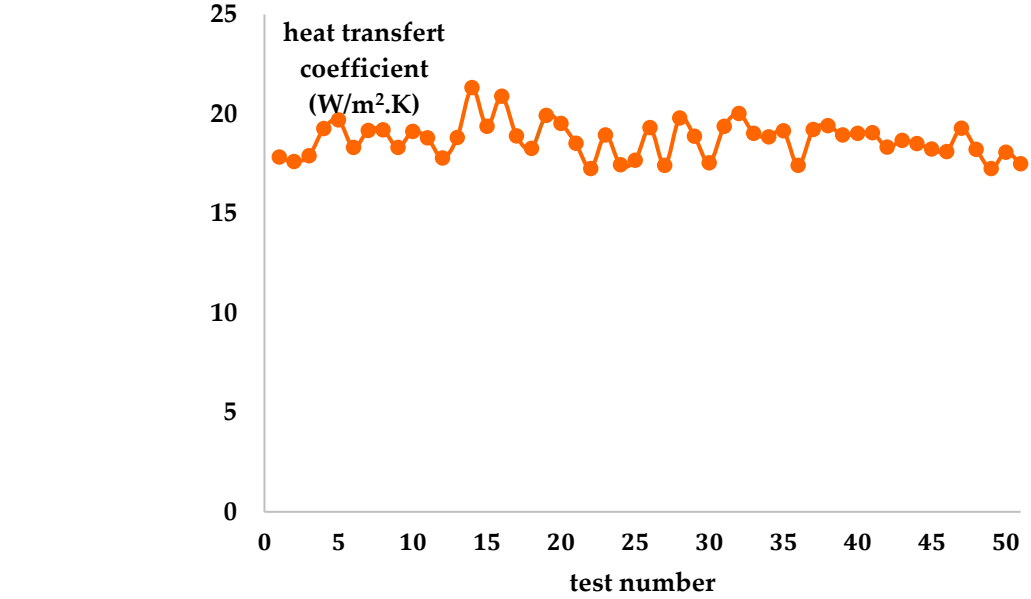

Figure 16. Estimation of the global heat transfer coefficient in the hot cell from temperatures measurements (thermocouples) and heat fluxes (flux meters measurements).

Figure 15 and Figure 16 shows the estimation of the global heat transfer coefficient in both, hot cell and cold cell, from temperatures measurements (thermocouples) and heat fluxes (flux meters measurements). The results are globally satisfactory, despite small variations between tests.

Finally, the uncertainties for the local convection heat transfer coefficient *h* are estimated (Table 3) and are globally satisfactory. An uncertainty of 5% was considered for flux meters and uncertainty of 0.02°C for thermocouples. It can be seen that the uncertainties are smaller in the hot cell as the fluxes and temperature differences involved are larger. It is in the cold cell, at the lower part of the wall, that the uncertainties are the greatest; at this point, the temperatures between the wall and the environment of the cold cell are very close and often of the order of a tenth of a degree.

Table 3 . Uncertainties for the local convection heat transfer coefficient.

Vertical position (m)	**cold cell**						**hot cell**					
	cavity of 5 mm for 10, 20, 30 flow rate ($m^3.h^{-1}$)			**cavity of 10 mm for 10, 20, 30 flow rate ($m^3.h^{-1}$)**			**cavity of 5 mm for 10, 20, 30 flow rate ($m^3.h^{-1}$)**			**cavity of 10 mm for 10, 20,30 flow rate ($m^3.h^{-1}$)**		
	10	**20**	**30**	**10**	**20**	**30**	**10**	**20**	**30**	**10**	**20**	**30**
0.8	1.5	1.5	1.7	1.5	1.4	1.7	1.5	1.5	1.4	1.8	1.8	1.6
0.56	2.7	2.3	2.7	2.2	2.0	2.4	1.2	1.2	1.1	1.3	1.3	1.2
0.345	4.6	3.0	3.0	3.1	2.7	3.2	1.5	1.6	1.5	1.6	1.6	1.4
0.125	5.1	2.8	2.7	3.1	2.9	3.4	1.4	1.3	1.5	1.4	1.5	1.2

Preprints (www.preprints.org) | NOT PEER-REVIEWED | Posted: 2 February 2021 doi:10.20944/preprints202102.0077.v1

3.3. Thermal performance of the ventilated wall

The objective of this study is to characterize the influence of the air space thickness and the air flow rate on the thermal performances of the ventilated wall. The thermal performance of the ventilated wall was evaluated through the pre-heating efficiency according to the equation (2) which represent the potentiality of the ventilatd wall in terms of its capability to pre-heat the air in the cavity [27].

$$E=(T_{inlet}-T_{out})\ /(T_{in}-T_{out}) \quad (2)$$

With :

- Tinlet : the supply air temperature measured in the top of the air cavity
- T_{out} is the outside air temperature (cold cell)
- T_{in} is the inside air temperature (hot cell).

Figure 17 shows the pre-heating efficiency of the ventilated wall**.** Experiments were carried out for differents air space thickness (5mm, 20 mm, 50 mm and 85 mm) and differents air flow rate (10 $m^3.h^{-1}$, 20 $m^3.h^{-1}$ and 30 $m^3.h^{-1}$). It can be seen that the pre-heating efficiency of the ventilated wall increase with the air space thickness. For an air flow 10 $m^3.h^{-1}$, the pre-heating efficiency of the ventilated wall increase from 57 % (for air space thickness of 5 mm) to 65 % (for air space thickness of 85 mm). It can be also seen that the pre-heating efficiency of the ventilated wall decrease with the air flow rate. For an air space thickness of 85 mm, the pre-heating efficiency of the ventilated wall decrease from 65 % (for an air flow rate 10 $m^3.h^{-1}$) to 54 % (for an air flow rate 30 $m^3.h^{-1}$).

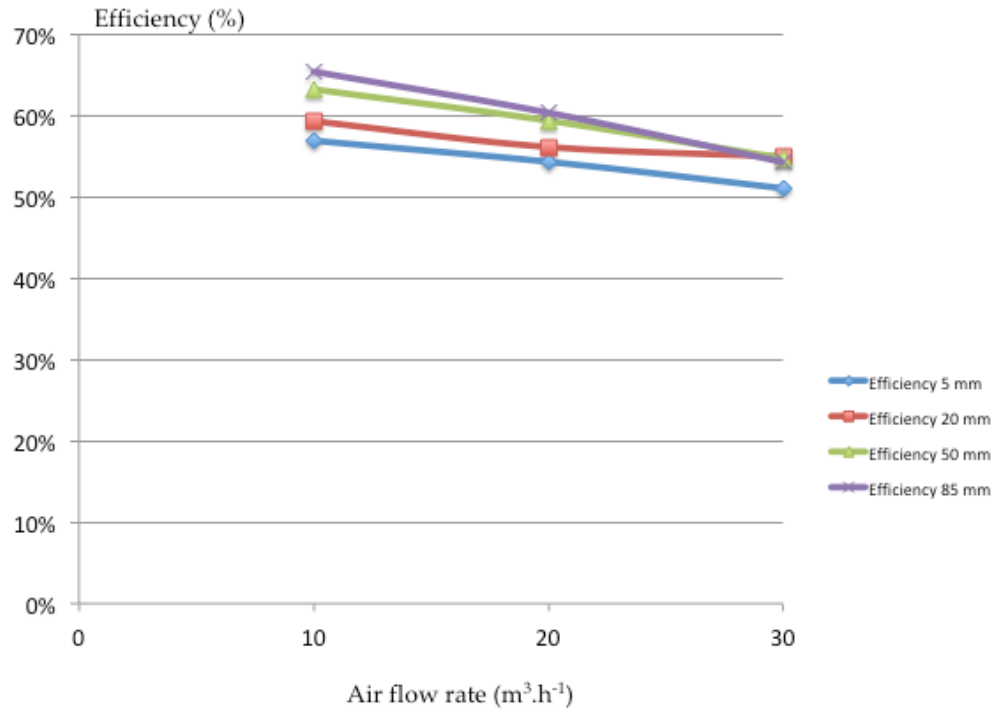

Figure 17. Pre-heating efficiency of the ventilated wall. Experiments were carried out for variable air space thickness (5mm, 20 mm, 50 mm and 85 mm) and variable air flow rate (10 $m^3.h^{-1}$, 20 $m^3.h^{-1}$ and 30 $m^3.h^{-1}$.)

4. Conclusion

This work describes an experimental study on the thermal performance of a ventilated bioclimatic wall. A ventilated wall prototype and an original Hot Box thermal metrology have been developed specifically. This paper presents the ventilated wall prototype, the experimental set-up and experimental results. The ambient temperature, the surface temperature of the ventilated prototype and the local heat transfer coefficients of the ventilated wall are measured. In addition, an uncertainty analysis on the local heat transfer coefficient is presented. Experimental results show that vertical position has a significant influence on the local heat transfer coefficient value. Finally, the influence of the air space thickness and the air flow rate on the thermal performances of the ventilated wall is studied. Results shows the pre-heating efficiency of the ventilated wall increase with the air space thickness and decrease with the air flow rate. These results shows, that the increase of the air space thickness of ventilated wall can be a solution to reduce the energy demands in buildings.

References

[1] Bâtiments à énergie positive et réduction carbone, (2019) 3–5. http://www.batiment-energiecarbone.fr/contexte-a2.html.

[2] E. Commission, Evaluation of the Energy Performance of Building Directive 2010/31/EU, 2015. http://ec.europa.eu/smart-regulation/evaluation/index_en.htm.

[3] T. Pflug, N. Nestle, T. Kuhn, M. Siroux, C. Maurer ,Modeling of facade elements with switchable U-value, Energy and Buildings, 164, (2018) 1-13.

[4] T. Pflug, B. Bueno, M. Siroux, T. Kuhn, Potential analysis of a new removable nsulation system, Energy and Buildings, 154, (2017), 391-403.

[5] C. Gregório-Atem, C. Aparicio-Fernández, H. Coch, JL. Vivancos, Opaque Ventilated Façade (OVF) Thermal Performance Simulation for Office Buildings in Brazil , Suistanability**, (2020)**, *12*(18), 7635; **https://doi.org/10.3390/su12187635**

[6] L.F. Cabeza, A. De Gracia, A. Castell, L. Navarro, E. Oro, Numerical modelling of ventilated facades : A review, 22 (2013) 539–549. https://doi.org/10.1016/j.rser.2013.02.029.

[7] H.Y. Chan, S.B. Riffat, J. Zhu, Review of passive solar heating and cooling technologies, Renew. Sustain. Energy Rev. 14 (2010) 781–789. https://doi.org/10.1016/j.rser.2009.10.030.

[8] C.M. Lai, S. Hokoi, Solar façades: A review, Build. Environ. 91 (2015) 152–165. https://doi.org/10.1016/j.buildenv.2015.01.007.

[9] S. Barbosa, K. Ip, Perspectives of double skin façades for naturally ventilated buildings: A review, Renew. Sustain. Energy Rev. 40 (2014) 1019–1029. https://doi.org/10.1016/j.rser.2014.07.192.

[10] A. Pappas, Z. Zhai, Numerical investigation on thermal performance and correlations of double skin façade with buoyancy-driven airflow, Energy Build. 40 (2008) 466–475. https://doi.org/10.1016/j.enbuild.2007.04.002.

[11] M.A. Shameri, M.A. Alghoul, K. Sopian, M.F.M. Zain, O. Elayeb, Perspectives of double skin façade systems in buildings and energy saving, Renew. Sustain. Energy Rev. 15 (2011) 1468–1475. https://doi.org/10.1016/j.rser.2010.10.016.

[12] G. Quesada, D. Rousse, Y. Dutil, M. Badache, S. Hallé, A comprehensive review of solar facades. Opaque solar facades, Renew. Sustain. Energy Rev. 16 (2012) 2820–2832. https://doi.org/10.1016/j.rser.2012.01.078.

[13] I. Cerón, E. Caamaño-Martín, F.J. Neila, "State-of-the-art" of building integrated photovoltaic products, Renew. Energy. 58 (2013) 127–133. https://doi.org/10.1016/j.renene.2013.02.013.

[14] O. Zogou, H. Stapountzis, Experimental validation of an improved concept of building integrated photovoltaic panels, Renew. Energy. 36 (2011) 3488–3498. https://doi.org/10.1016/j.renene.2011.05.034.

[15] D.J. Harris, N. Helwig, Solar chimney and building ventilation, Appl. Energy. 84 (2007) 135–146. https://doi.org/10.1016/j.apenergy.2006.07.001.

[16] R. Khanal, C. Lei, Solar chimney-A passive strategy for natural ventilation, Energy Build. 43 (2011) 1811–1819. https://doi.org/10.1016/j.enbuild.2011.03.035.

[17] O. Saadatian, K. Sopian, C.H. Lim, N. Asim, M.Y. Sulaiman, Trombe walls: A review of opportunities and challenges in research and development, Renew. Sustain. Energy Rev. 16 (2012) 6340–6351. https://doi.org/10.1016/j.rser.2012.06.032.

[18] A. Alaidroos, M. Krarti, Experimental validation of a numerical model for ventilated wall cavity with spray evaporative cooling systems for hot and dry climates, Energy and Buildings 131 (2016) 207–222. https://doi.org/10.1016/j.enbuild.2016.09.035.

[19] O. Aleksandrowicz, A. Yezioro, Mechanically ventilated double-skin facade in a hot and humid climate: summer monitoring in an office tower in Tel Aviv, Archit. Sci. Rev. 61 (2018) 171–188. https://doi.org/10.1080/00038628.2018.1450726.

[20] Wang, Q. Du, C. Zhang, X. Xu, Energy Performance of Triple Glazed Window with Built-in Venetian Blinds by Utilizing Forced Ventilated airflow, Procedia Eng. 205 (2017) 3993–4000. https://doi.org/10.1016/j.proeng.2017.09.865.

[21] L. C. O. Souza, H. A. Souza, E. F. Rodrigues, Experimental and numerical analysis of a naturally ventilated double-skin façade, Energy Build. 165 (2018) 328–339. https://doi.org/10.1016/j.enbuild.2018.01.048.

[22] J. Parra, A. Guardo, E. Egusquiza, P. Alavedra, Thermal performance of ventilated double skin façades with venetian blinds, Energies. 8 (2015) 4882–4898. https://doi.org/10.3390/en8064882.

[23] G. Michaux, R. Greffet, P. Salagnac, J.B. Ridoret, Modelling of an airflow window and numerical investigation of its thermal performances by comparison to conventional double and triple-glazed windows, Appl. Energy. 242 (2019) 27–45. https://doi.org/10.1016/j.apenergy.2019.03.029.

[24] F. Gloriant, A. Joulin, P. Tittelein, S. Lassue, Using heat flux sensors for a contribution to experimental analysis of heat transfers on a triple-glazed supply-air window, Energy. 215 (2021) 119154. https://doi.org/10.1016/j.energy.2020.119154.

[25] D. Sukamto, F. Gloriant, M. Siroux, Mise en place d 'un dispositif expérimental pour la caractérisation énergétique d'une paroi bioclimatique ventilée Conférence SFT Belfort Therm. Mix Énergétique, 2020: pp. 1–8. https://doi.org/10.25855/SFT2020-037.

[26] J. Padet, Convection thermique et massique Principes généraux, 33 (2005) 0–23. https://www-techniques-ingenieur-fr.ezproxy.insa-strasbourg.fr/base-documentaire/energies-th4/transferts-thermiques-42214210/convection-thermique-et-massique-be8205/.

[27] S. Fantuccia, V. Serraa, M. Perino, Dynamic insulation systems: experimental analysis on a parietodynamic wall, Energy Procedia 78 (2015) 549 – 554.

 doi:10.20944/preprints202102.0077.v1

Author Contributions: Conceptualization, D.S and M.S; methodology, D.S., M.S and F. G.; investigation D.S., M.S and F. G. writing—original draft preparation D.S., M.S and F. G., writing—review and editing D. S. M.S and F.G.. All authors have read and agreed to the published version of the manuscript.

Funding: This research was funded by Arconic Foundation and by the Ministry of higher education of Republic of Indonesia.

Acknowledgments: The authors acknowledge the financial contribution of the Arconic Foundation and the Ministry of higher education of Republic of Indonesia.

Conflicts of Interest: The authors declare no conflict of interest.